Rapid Water Disinfection Using Vertically Aligned MoS₂ Nanofilms and Visible Light

Chong Liu[1], Desheng Kong[1], Po-Chun Hsu[1], Hongtao Yuan[1], Hyun-Wook Lee[1], Yayuan Liu[1], Haotian Wang[2], Shuang Wang[3], Kai Yan[1], Dingchang Lin[1], Peter A. Maraccini[4], Kimberly M. Parker[4], Alexandria B. Boehm[4], Yi Cui[*1,5]

[1] *Department of Materials Science and Engineering, Stanford University, Stanford, California 94305, USA*

[2] *Department of Applied Physics, Stanford University, Stanford, California 94305, USA*

[3] *Department of Electrical Engineering, Stanford University, Stanford, California 94305, USA*

[4] *Department of Civil and Environmental Engineering, Stanford University, Stanford, California 94305, USA*

[5] *Stanford Institute for Materials and Energy Sciences, SLAC National Accelerator Laboratory, 2575 Sand Hill Road, Menlo Park, California 94305, USA*

*Correspondence should be addressed to Y.C. (yicui@stanford.edu)

Solar energy is readily available in most climates and can be used for water purification. However, solar disinfection of drinking water (SODIS) mostly relies on ultraviolet light, which represents only 4% of total solar energy, and this leads to slow treatment speed. The development of new materials that can harvest visible light for water disinfection, and speed up solar water purification, is therefore highly desirable. Here, we show that few-layered vertically aligned MoS_2 (FLV-MoS_2) films can be used to harvest the whole spectrum of visible light (~ 50% of solar energy) and achieve highly efficient water disinfection. The bandgap of MoS_2 was increased from 1.3 eV to 1.55 eV by decreasing the domain size, which allowed the FLV-MoS_2 to generate reactive oxygen species (ROS) for bacterial inactivation in water. The FLV-MoS_2 showed ~15 times better log inactivation efficiency of indicator bacteria compared to bulk MoS_2, and much faster inactivation of bacteria under both visible light and sunlight illumination compared to widely used TiO_2. Moreover, by using a 5 nm copper film on top of the FLV-MoS_2 as a catalyst to facilitate electron-hole pair separation and promote the generation of ROS, the disinfection rate was further increased 6 fold. With our approach, we achieved water disinfection of >99.999% inactivation of bacteria in 20 minutes with a small amount of material (1.6 mg/L) under simulated visible light.

Rapid and energy-efficient water disinfection methods are urgently required to address global challenges related to energy and water scarcity[1-5]. Solar energy is an attractive renewable energy resource and can be used for water disinfection via solar disinfection of drinking water (SODIS), an approach employed throughout the world, particularly in developing countries lacking potable water distribution systems, for disinfecting water for consumption[6]. Sunlight can inactivate microorganisms via direct or indirect mechanisms. Direct mechanisms involve photons (usually

UVB or UVA) directly interacting with nucleic acids or other essential macromolecules to cause inactivation. Indirect mechanisms involve photons (UV or visible) interacting with chromophores either within the organism or external to the organism to create reactive oxygen species (ROS) that subsequently cause inactivation. To date, most studies suggest the disinfection by UV photons is one of the most important means of inactivating waterborne pathogens[7-9]. However, energy in UVA and UVB collectively only account for 4% of the energy in the solar spectrum, so SODIS is time-consuming (requires 6-48 hours exposure time)[6]. It would be desirable to more effectively harness energy in photons from the visible range to speed up photoinactivation. One way is to use a semiconductor-based photocatalyst[10-12]. When a photocatalyst absorbs light, it generates electron-hole pairs so that electrons and holes can react with water and dissolved oxygen separately to generate ROS. ROS, such as hydroxyl radical, singlet oxygen, and superoxide, are strong oxidants and can disinfect pathogens by damaging essential macromolecules [13, 14]. Technically, the potentials (vs. Normal Hydrogen Electrode (NHE)) for ROS production (pH 7) at the electron side for oxygen reductions are -0.33 V ($O_2/\bullet O_2^-$), 0.28 V (O_2/H_2O_2) and at the hole side for water oxidation are 1.1-1.9 V ($H_2O/OH\bullet$), 0.82 V (H_2O/O_2)[15-18] (Fig. 1a) so that it is possible for an efficient photocatalyst to use the whole visible light range of solar spectrum. However, the bandgap of the most studied metal oxide photocatalysts are typically too large so most of the visible part of the solar spectrum is not utilized. For example, TiO_2 has a bandgap of 3.0-3.2 eV and only harvests UV light[19]. Lowering the bandgap of TiO_2 and enabling its absorption of visible light usually involves complex synthesis such as doping with N, S or Fe[19-24], making hybrid composites with lower bandgap materials[25, 26] and advanced structural design[27, 28] which limits its practical application for photocatalytic applications[29, 30]. Besides lowering the bandgap of metal oxides, research has investigated the potential for new semiconductor materials with small bandgap such as C_3N_4 (2.7eV, cutoff wavelength 459 nm)[31, 32], red phosphorus (1.42 eV, cutoff wavelength 873 nm)[33] as photocatalysts that utilize visible light. The disinfection efficacy, specifically the disinfection rate, of these materials is still far

3

from practical application [25, 31, 34-37]. Seeking novel photocatalysts that can harvest visible light for fast water disinfection are extremely attractive.

MoS_2, a prototypical layered transition metal dichalcogenide (TMD), is an emerging semiconductor material with physical and chemical properties conducive to applications in transistors, electrocatalysts for hydrogen evolution reaction[38-42]. Single or few-layered sheets of MoS_2 exhibit intriguing properties distinct from bulk MoS_2. By decreasing the thickness of MoS_2 to few layers or single layer, its bandgap changes from an indirect bandgap of 1.3 eV to a direct bandgap of 1.9 eV[43]. Also, nanostructured MoS_2 would benefit the separation of electron-hole pairs by decreasing the distances for electrons and holes to diffuse to the surface of the materials and also increase the reaction sites[44]. Here we report the successful use of few layered vertically aligned MoS_2 (FLV-MoS_2) as a photocatalyst for water disinfection under visible light illumination (Fig. 1b). The FLV-MoS_2 has great potential for photocatalytic water disinfection owing to its low-cost and straightforward synthesis. FLV-MoS_2 showed much faster disinfection than TiO_2 under both visible light and sunlight illumination. Because semiconductor materials are nonspecific in catalyzing ROS production among other competing reactions (such as hydrogen evolution, oxygen reduction and oxidation), to promote the production of ROS, additional catalysts Cu or Au were deposited onto the MoS_2 films. With 5 nm of Cu or Au as reaction catalysts as well as to facilitate the separation of electron-hole pairs, FLV-MoS_2 achieved rapid water disinfection with 5 log (>99.999%) inactivation of *Escherichia coli* within 20 min or 60 min, respectively, comparing to pristine FLV-MoS_2 of 120 min.

Growth and characterization of FLV-MoS₂.

The FLV-MoS$_2$ was grown by first sputtering Mo film on glassy carbon (GC) substrate and then sulfurize at 500 °C for 10 min[41]. The sulfurization was conducted in a sulfur-rich environment and the MoS$_2$ film thickness was determined by the initial thickness of Mo film sputtered. The transmission electron microscopy (TEM) images of the 40 nm MoS$_2$ film are shown in Fig. 2a. It is clear that the as-grown MoS$_2$ film is composed of vertically aligned layers of MoS$_2$ with domain sizes around 3-10 layers as also shown in our previous studies[41, 42]. Reports have demonstrated that MoS$_2$ has higher in-plane electrical conductivity[40, 41] and also higher catalytic activity on the edge sites, which means this vertically-aligned structure can have better electron-hole transport from MoS$_2$ to electrolytes. For photoelectrochemical reactions, the material band structure is the key factor that directly determines the mechanism, products, and efficiency. Therefore, the properties of the vertically-aligned MoS$_2$ were characterized. First, the bandgap was characterized by measuring the absorption spectrum of MoS$_2$. The absorption spectra of 40 nm MoS$_2$ are shown in Fig. 2b. The bandgap value was extracted from the relation between absorption coefficient and photon energy for the indirect bandgap semiconductor. The plot of $(\alpha h\upsilon)^{1/2}$ versus $h\upsilon$ is shown in Supplementary Fig. 1. The bandgap extraction gives 1.55 eV for 40 nm FLV-MoS$_2$. This allows FLV-MoS$_2$ to absorb light up to 800 nm wavelength and the solar spectrum utilization is also increased to ~50% in energy comparing to TiO$_2$ of 4%. The Fermi level of FLV-MoS$_2$ was characterized by scanning Kelvin probe force microscopy and the results are shown in Fig. 2c-e. Au line was patterned on the MoS$_2$ film as a reference because it has a stable work function of 5.1 eV. Fig. 2d shows the line scan data on the MoS$_2$ film crossing the Au pattern. The Fermi level of MoS$_2$ on the line scan ranges from 5.23 to 5.26 eV with an average of 5.24 eV. The Fermi level mapping on a 1.5×12 mm^2 area in Fig. 2e shows the uniformity of the as-grown FLV-MoS$_2$ film and the averaging Fermi level across the entire area is ~5.24 eV. The valence band position of FLV-MoS$_2$ was confirmed to be 5.55 eV using ultraviolet photoelectron spectroscopy (UPS) and the results are shown in Supplementary Fig. 2. Hence, the band position of FLV-MoS$_2$ with respect to ROS reaction potential and also band position of bulk MoS$_2$ are

shown in Fig. 2f. The valence band position for bulk MoS_2 is 5.54 eV (Supplementary Fig. 2). It is clear that FLV-MoS_2 is suitable for ROS generation for photocatalytic water disinfection.

Photocatalytic disinfection performance of FLV-MoS_2.

The photocatalytic disinfection performance of FLV-MoS_2 was then examined. Firstly, the photocatalytic effect of FLV-MoS_2 was confirmed by comparing the inactivation efficiencies of bacteria with FLV-MoS_2 under visible light (without UVA and UVB) to those of the controls consisting of FLV-MoS_2 incubated with bacteria in the dark and visible light illumination of the bacterial suspension without FLV-MoS_2. A solar simulator equipped with a UV-blocking filter was used as the light source. The Gram negative bacterium *Escherichia coli* was used as a process indicator in all experiments unless otherwise specified. Bacterial concentration at each time point of the experiment was normalized to the starting concentration at time 0 and the results are shown in Fig. 3a. Visible light alone or FLV-MoS_2 in the dark both showed <50% disinfection efficiency after 120 min while FLV-MoS_2 under visible light showed >99.999% *E. coli* inactivation in 120 min after which bacteria could not be detected and no recovery was observed (Supplementary Fig. 3). The disinfection efficiency of FLV-MoS_2 was also compared to that of an equal mass of bulk MoS_2 (suspended flakes of ~2 µm) under the same experimental condition (Fig. 3b). Bulk MoS_2 showed 54% efficiency over 120 min which is much lower than that of FLV-MoS_2 of >99.999%. This suggests that decreasing the size of MoS_2 to only few layers (~ 2-6 nm thick) can increase the photocatalyst properties of MoS_2. Decreasing the layer thickness of MoS_2 increases ROS generation due to both the bandgap widening and diffusion distance shortening for electrons and holes to material surface. Also, the disinfection performance was compared between equal mass of FLV-MoS_2 and horizontal MoS_2 film (Fig. 3b). The horizontal MoS_2 film was made of stacked MoS_2 nano flakes with each flake 1-6 nm in thickness. Since both samples have larger bandgap than bulk MoS_2, the disinfection rates were much higher.

6

Between the FLV-MoS$_2$ and horizontal MoS$_2$, the vertical direction configuration gave higher disinfection rate. This could be owing to a higher in-plane conductivity of electron/hole in MoS$_2$ and also more active edge sites exposed on the FLV-MoS$_2$ film.

To eliminate the thermal effect potentially caused by infrared (IR) light, the disinfection efficiency of *E. coli* in water with FLV-MoS$_2$ under visible light combined with IR light and under only IR light was compared. The light spectrum is shown in Fig. 3c and the disinfection performance is shown in Fig. 3d. With IR light alone, the disinfection efficiency (83%) was much less than that of visible light combined with IR light together (>99.999%). Additionally, a temperature control experiment also eliminated the thermal effect (Supplementary Fig. 5). Therefore it is confirmed that visible light photocatalysis instead of thermal effect induces most of the disinfection. The disinfection effect of FLV-MoS$_2$ on a model Gram positive bacterium, *Enterococcus faecalis*, and another strain of *E. coli* was also demonstrated. No live bacteria was detected after 120 min of illumination (Supplementary Fig. 6 and Supplementary Fig. 7). This suggests that FLV-MoS$_2$ can be used to inactivate a variety of bacteria.

The disinfection performance of FLV-MoS$_2$ was compared with the well-studied photocatalyst TiO$_2$. TiO$_2$ film was grown through atomic layer deposition method following an annealing process. The thickness of TiO$_2$ was kept the same as FLV-MoS$_2$. The Raman spectroscopy of both FLV-MoS$_2$ and TiO$_2$ are shown in Fig. 3e and TiO$_2$ was confirmed to be in anatase phase. The comparison of disinfection performances of FLV-MoS$_2$ and TiO$_2$ are shown in Fig. 3f. Due to the large 3.2 eV bandgap of TiO$_2$ (corresponding to light wavelength of 387 nm), illumination under the solar spectrum with UV light filter did not induce any photocatalytic ROS generation. Hence *E. coli* concentration just decreased 44% after 120 min of illumination which is similar to

that of the light control. This confirms that TiO_2 was unable to harvest visible light for photocatalytic water disinfection. Using real sunlight as the light source (13:00 local time, March 30 2013, Stanford, California, USA; spectrum is in Supplementary Fig. 8), the disinfection performance of FLV-MoS_2 and TiO_2 were also compared (Fig. 3f). FLV-MoS_2 showed 5 log inactivation of bacteria concentration (>99.999% inactivation efficiency) and no live bacteria was detected within 60 min of real sunlight illumination. This gives a first order disinfection rate of 0.18 min^{-1} (R^2=0.99) for FLV-MoS_2 under real sunlight. TiO_2 showed a log inactivation efficiency of 3 log (99.9%) in 60 min corresponding to a disinfection rate of 0.12 min^{-1} (R^2=0.96). Thus, the photocatalytic effect of FLV-MoS_2 was much better than TiO_2 for *E. coli* disinfection under both visible light and real sunlight.

Disinfection performance enhanced by additional catalysts.

Normally, the performance of a photocatalyst is governed by two critical properties which are 1) the utilization of solar spectrum by the semiconductor photocatalyst and 2) the efficacy of the generated electron-hole pairs for ROS production. For the second property, there is competition between the generated electrons and holes to produce ROS and other physical processes such as electron-hole recombination, trapping in the material during diffusion, as well as participating in other reactions (such as hydrogen evolution, oxygen reduction and oxidation). Semiconductor materials are usually nonspecific in catalyzing ROS production. Hence to promote the production of ROS, addition of catalysts is crucial. Nano-sized noble metals are used to decorate the semiconductor material surface to serve as ROS catalysts and to form metal-semiconductor junctions to enhance the electron hole separation. It has been shown in the literature that with the addition of nano sized noble metals, ROS production can be increased dramatically[45-47].

To accelerate the photocatalytic disinfection rate, 5 nm of Cu or Au was deposited onto the FLV-MoS$_2$ to catalyze ROS generation and also improve electron-hole pair separation. Cu and Au are good catalysts for ROS generation and they preferentially catalyze two electron oxygen reduction reaction for H$_2$O$_2$ generation over a four electron transfer reaction (Supplementary Fig. 9). Cu and Au are deposited via thermal evaporation process. The morphologies of as-grown Cu-MoS$_2$ and Au-MoS$_2$ were characterized by TEM and scanning electron microscopy (SEM) and the images are shown in Fig. 4a and Supplementary Fig. 10. The thermal evaporation process did not change the morphology of MoS$_2$ film. No obvious intercalation of Cu or Au were observed because the layer spacing was ~0.63 nm and ~0.62 nm for Cu-MoS$_2$ and Au-MoS$_2$, respectively, which is similar to pristine FLV-MoS$_2$ of ~0.60 nm (Supplementary Fig. 11). The existence of Cu and Au film was confirmed by X-ray photoelectron spectroscopy (XPS) (Fig. 4b). The XPS data showed signature peaks for Cu 2p$_{3/2}$ at 932.6 eV and for Au 4f$_{7/2}$ at 83.9 eV. Besides the catalytic effect, Cu and Au can also increase the separation of electron-hole pairs. The work function of Cu and Au is 4.7 eV and 5.1 eV, respectively. When in contact with p-type FLV-MoS$_2$, the Schottky junction facilitates the electron migration to Cu or Au surface and participate in oxygen reduction reactions to produce ROS as explained in the schematic in Fig. 4c. This should further promote the oxygen reduction reaction for ROS generation. The disinfection performances of Cu-MoS$_2$ and Au-MoS$_2$ are shown in Fig. 4d. A solar simulator with a UV light filter was used as light source as in the disinfection experiments. For FLV-MoS$_2$ without any catalyst, after 120 min of illumination, no live *E. coli* was detected. With 5 nm of Cu, the disinfection rate was enhanced and within only 20 min, no live bacteria was detected, which is equivalent to a disinfection efficiency of >99.999%. For the Au-MoS$_2$, the illumination time to achieve >99.999% disinfection efficiency was also shortened relative to FLV-MoS$_2$ to 60 min. The disinfection rate for Cu-MoS$_2$ and Au-MoS$_2$ was 0.57 min^{-1} (R^2=0.99) and 0.19 min^{-1} (R^2=0.96), respectively, under solar simulator with UV light filter. It is much faster compared to FLV-MoS$_2$ of 0.087 min^{-1} (R^2=0.99). The disinfection enhancement confirmed the efficacy of Cu and Au to separate

electron-hole pair more efficiently and catalyze the oxygen reduction reactions for ROS generation. With Cu and Au as catalysts the disinfection rate is enhanced 6 fold and 2 fold, respectively. After photocatalytic disinfection experiment, the concentration of Cu or Au was measured. No detectable Au was present in water sample and Cu concentration was 3.25 ppb (μg/L) which is < 1% the Cu catalyst mass loading.

Photocatalytic disinfection mechanism.

Furthermore, to directly prove the disinfection mechanism by ROS in FLV-MoS_2 and Cu-MoS_2 systems and also to prove the catalytic effect of Cu, ROS concentrations in both systems were measured and a series of ROS scavenging experiments were conducted. The results are shown in Supplementary Fig. 12-14 and Supplementary Discussion. It is showed that four ROS (O_2^-, $^1O_2$, H_2O_2 and OH•) were present in both FLV-MoS_2 and Cu-MoS_2 system with concentration of H_2O_2> •O_2^-> $^1O_2$ > OH•. Moreover, for each ROS, the concentration in Cu-MoS_2 system is higher than that in FLV-MoS_2 system. This is consistent with the fact that Cu-MoS_2 demonstrated a higher disinfection rate and also proves the effectiveness of Cu in catalyzing ROS generation. Six scavenger quenching experiments were conducted to study the disinfection contribution of each ROS as well as electron and hole. The results suggested that H_2O_2 has the strongest effect in inactivating bacteria and oxygen reduction related ROS dominates the disinfection effect. All these results are consistent with the band structure of MoS_2 which favors the oxygen reduction to produce ROS. Besides, the FLV-MoS_2 and Cu-MoS_2 were proven to be stable after multi-cycle tests (Supplementary Fig. 15).

The bacterial disinfection performance of Cu-MoS_2, with disinfection rate of 0.57 min^{-1} (R^2=0.99), under solar simulator with a UV filter is so far among the best based on a review of the literature

in terms of speed and log reduction in bacterial concentration (Fig. 4e and Supplementary Table 1). Compared with those achieving total disinfection (no live bacteria detected) within 30 min, such as ZnO/Cu[48], GO-CdS[34] and SGO-ZnO-Ag[35], the material mass loading used in the case of Cu-MoS$_2$ is ~60 times less than the others. On the other hand, for fixed photocatalysts grown on substrates with similar material mass loading such as TiO$_2$-CdS[25], the disinfection rate of Cu-MoS$_2$ (>99.999%) is much faster than that of TiO$_2$-CdS (~90%) in 20 min. Hence Cu-MoS$_2$ shows a great advantage as a new effective visible light photocatalyst for water disinfection.

In conclusion, we demonstrated efficient harvesting of visible light for photocatalytic water disinfection with a novel material, FLV-MoS$_2$. By decreasing the domain size, the bandgap of MoS$_2$ was increased from 1.3 eV (bulk material) to 1.55 eV (FLV-MoS$_2$). It enabled the FLV-MoS$_2$ to successful generate ROS for bacteria inactivation in water. The FLV-MoS$_2$ showed faster disinfection than most studied TiO$_2$. With additional deposition of Cu and Au to assist electron-hole pair separation and also catalyze ROSs production reactions, FLV-MoS$_2$ showed rapid inactivation of >99.999% bacteria in only 20 min and 60 min, respectively. The promising performance of FLV-MoS$_2$ and Cu-MoS$_2$ on bacteria shows great potential for them as photocatalyst for visible light pathogen (bacteria, viruses and protozoa) inactivation in water.

References

1. Shannon, M.A. et al. Science and technology for water purification in the coming decades. *Nature* **452**, 301-310 (2008).
2. Schwarzenbach, R.P. et al. The challenge of micropollutants in aquatic systems. *Science* **313**, 1072-1077 (2006).
3. Liu, C. et al. Conducting nanosponge electroporation for affordable and high-efficiency disinfection of bacteria and viruses in water. *Nano Lett.* **13**, 4288-4293 (2013).
4. Liu, C. et al. Static electricity powered copper oxide nanowire microbicidal electroporation for water disinfection. *Nano Lett.* **14**, 5603-5608 (2014).
5. Logan, B.E. & Elimelech, M. Membrane-based processes for sustainable power generation using water. *Nature* **488**, 313-319 (2012).
6. McGuigan, K.G. et al. Solar water disinfection (SODIS): A review from bench-top to roof-top. *J. Hazard. Mater.* **235**, 29-46 (2012).
7. Sinha, R.P. & Hader, D.P. UV-induced DNA damage and repair: a review. *Photochem. Photobiol. Sci.* **1**, 225-236 (2002).
8. Hijnen, W.A.M., Beerendonk, E.F. & Medema, G.J. Inactivation credit of UV radiation for viruses, bacteria and protozoan (oo)cysts in water: A review. *Water Res.* **40**, 3-22 (2006).
9. Silverman, A.I., Peterson, B.M., Boehm, A.B., McNeill, K. & Nelson, K.L. Sunlight inactivation of human viruses and bacteriophages in coastal waters containing natural photosensitizers. *Environ. Sci. Technol.* **47**, 1870-1878 (2013).
10. Dong, S.Y. et al. Recent developments in heterogeneous photocatalytic water treatment using visible light-responsive photocatalysts: a review. *Rsc Adv.* **5**, 14610-14630 (2015).
11. Dong, S.Y. et al. Designing three-dimensional acicular sheaf shaped $BiVO_4$/reduced graphene oxide composites for efficient sunlight-driven photocatalytic degradation of dye wastewater. *Chem. Eng. J.* **249**, 102-110 (2014).
12. Dong, S.Y. et al. $ZnSnO_3$ hollow nanospheres/reduced graphene oxide nanocomposites as high-performance photocatalysts for degradation of metronidazole. *Appl. Catal., B* **144**, 386-393 (2014).
13. Chong, M.N., Jin, B., Chow, C.W.K. & Saint, C. Recent developments in photocatalytic water treatment technology: A review. *Water Res.* **44**, 2997-3027 (2010).
14. Malato, S., Fernandez-Ibanez, P., Maldonado, M.I., Blanco, J. & Gernjak, W. Decontamination and disinfection of water by solar photocatalysis: Recent overview and trends. *Catal. Today* **147**, 1-59 (2009).
15. Wardman, P. Reduction potentials of one-electron couples involving free-radicals in aqueous-solution. *Journal of Physical and Chemical Reference Data* **18**, 1637-1755 (1989).
16. Wood, P.M. The potential diagram for oxygen at pH-7. *Biochem. J.* **253**, 287-289 (1988).
17. Lawless, D., Serpone, N. & Meisel, D. Role of OH. radicals and trapped holes in photocatalysis - a pulse radiolysis study. *J. Phys. Chem.* **95**, 5166-5170 (1991).
18. Liao, H.D. & Reitberger, T. Generation of free OH_{aq} radicals by black light illumination of Degussa (Evonik) P25 TiO_2 aqueous suspensions. *Catalysts* **3**, 418-443 (2013).
19. Chen, X. & Mao, S.S. Titanium dioxide nanomaterials: Synthesis, properties, modifications, and applications. *Chem. Rev.* **107**, 2891-2959 (2007).
20. Li, Q., Xie, R.C., Ll, Y.W., Mintz, E.A. & Shang, J.K. Enhanced visible-light-induced photocatalytic disinfection of E-coli by carbon-sensitized nitrogen-doped titanium oxide. *Environ. Sci. Technol.* **41**, 5050-5056 (2007).

21. Cong, Y., Zhang, J.L., Chen, F., Anpo, M. & He, D.N. Preparation, photocatalytic activity, and mechanism of Nano-TiO_2 co-doped with nitrogen and iron (III). *J. Phys. Chem. C* **111**, 10618-10623 (2007).

22. Asahi, R., Morikawa, T., Ohwaki, T., Aoki, K. & Taga, Y. Visible-light photocatalysis in nitrogen-doped titanium oxides. *Science* **293**, 269-271 (2001).

23. Choi, J., Park, H. & Hoffmann, M.R. Effects of single metal-ion doping on the visible-light photoreactivity of TiO_2. *J. Phys. Chem. C* **114**, 783-792 (2010).

24. Yu, J.C. et al. Efficient visible-light-induced photocatalytic disinfection on sulfur-doped nanocrystalline titania. *Environ. Sci. Technol.* **39**, 1175-1179 (2005).

25. Hayden, S.C., Allam, N.K. & El-Sayed, M.A. TiO_2 nanotube/CdS hybrid electrodes: extraordinary enhancement in the inactivation of *Escherichia coli*. *J. Am. Chem. Soc.* **132**, 14406-14408 (2010).

26. Chen, C. et al. Synthesis of visible-light responsive graphene oxide/TiO_2 composites with p/n heterojunction. *Acs Nano* **4**, 6425-6432 (2010).

27. Yu, J.G., Dai, G.P. & Huang, B.B. Fabrication and characterization of visible-light-driven plasmonic photocatalyst Ag/AgCl/TiO_2 TiO_2 nanotube arrays. *J. Phys. Chem. C* **113**, 16394-16401 (2009).

28. Mor, G.K., Varghese, O.K., Paulose, M., Shankar, K. & Grimes, C.A. A review on highly ordered, vertically oriented TiO_2 nanotube arrays: Fabrication, material properties, and solar energy applications. *Solar Energy Materials and Solar Cells* **90**, 2011-2075 (2006).

29. Tao, J.G., Luttrell, T. & Batzill, M. A two-dimensional phase of TiO_2 with a reduced bandgap. *Nat. Chem.* **3**, 296-300 (2011).

30. Dette, C. et al. TiO_2 anatase with a bandgap in the visible region. *Nano Lett.* **14**, 6533-6538 (2014).

31. Huang, J.H., Ho, W.K. & Wang, X.C. Metal-free disinfection effects induced by graphitic carbon nitride polymers under visible light illumination. *Chem. Commun.* **50**, 4338-4340 (2014).

32. Wang, X.C. et al. A metal-free polymeric photocatalyst for hydrogen production from water under visible light. *Nat. Mater.* **8**, 76-80 (2009).

33. Xia, D.H. et al. Red phosphorus: an earth-abundant elemental photocatalyst for "green" bacterial inactivation under visible light. *Environ. Sci. Technol.* **49**, 6264-6273 (2015).

34. Gao, P., Liu, J.C., Sun, D.D. & Ng, W. Graphene oxide-CdS composite with high photocatalytic degradation and disinfection activities under visible light irradiation. *J. Hazard. Mater.* **250**, 412-420 (2013).

35. Gao, P., Ng, K. & Sun, D.D. Sulfonated graphene oxide-ZnO-Ag photocatalyst for fast photodegradation and disinfection under visible light. *J. Hazard. Mater.* **262**, 826-835 (2013).

36. Wang, W.J. et al. Visible-light-driven photocatalytic inactivation of *E. coli* K-12 by bismuth vanadate nanotubes: bactericidal performance and mechanism. *Environ. Sci. Technol.* **46**, 4599-4606 (2012).

37. Wang, W.J., Yu, J.C., Xia, D.H., Wong, P.K. & Li, Y.C. Graphene and g-C_3N_4 nanosheets cowrapped elemental alpha-sulfur as a novel metal-free heterojunction photocatalyst for bacterial inactivation under visible-light. *Environ. Sci. Technol.* **47**, 8724-8732 (2013).

38. Radisavljevic, B., Radenovic, A., Brivio, J., Giacometti, V. & Kis, A. Single-layer MoS_2 transistors. *Nat. Nanotechnol.* **6**, 147-150 (2011).

39. Wang, Q.H., Kalantar-Zadeh, K., Kis, A., Coleman, J.N. & Strano, M.S. Electronics and optoelectronics of two-dimensional transition metal dichalcogenides. *Nat. Nanotechnol.* **7**, 699-712 (2012).

40.   Jaramillo, T.F. et al. Identification of active edge sites for electrochemical H_2 evolution from MoS_2 nanocatalysts. *Science* **317**, 100-102 (2007).

41.   Kong, D.S. et al. Synthesis of MoS_2 and $MoSe_2$ films with vertically aligned layers. *Nano Lett.* **13**, 1341-1347 (2013).

42.   Wang, H.T. et al. Electrochemical tuning of vertically aligned MoS_2 nanofilms and its application in improving hydrogen evolution reaction. *Proc. Natl. Acad. Sci. U. S. A.* **110**, 19701-19706 (2013).

43.   Mak, K.F., Lee, C., Hone, J., Shan, J. & Heinz, T.F. Atomically thin MoS_2: a new direct-gap semiconductor. *Phys. Rev. Lett.* **105** (2010).

44.   Tong, H. et al. Nano-photocatalytic Materials: Possibilities and Challenges. *Adv. Mater.* **24**, 229-251 (2012).

45.   Sakthivel, S. et al. Enhancement of photocatalytic activity by metal deposition: characterisation and photonic efficiency of Pt, Au and Pd deposited on TiO2 catalyst. *Water Res.* **38**, 3001-3008 (2004).

46.   Li, H.X. et al. Mesoporous Au/TiO2 nanocomposites with enhanced photocatalytic activity. *J. Am. Chem. Soc.* **129**, 4538-4539 (2007).

47.   Subramanian, V., Wolf, E.E. & Kamat, P.V. Catalysis with TiO_2/gold nanocomposites. Effect of metal particle size on the Fermi level equilibration. *J. Am. Chem. Soc.* **126**, 4943-4950 (2004).

48.   Bai, H.W., Liu, Z.Y. & Sun, D.D. Hierarchical ZnO/Cu "corn-like" materials with high photodegradation and antibacterial capability under visible light. *Phys. Chem. Chem. Phys.* **13**, 6205-6210 (2011).

Acknowledgements

Author Contributions

C.L. and Y.C. conceived the concept. C.L. synthesized the samples and conducted the disinfection measurement and material characterizations. D. K. and H. W. helped with material synthesis. P.-C. H. and S. W. helped with the optical measurement. H. Y. helped with Kelvin Probe measurement. H. L. did the TEM characterization. D. K. helped with Raman Spectroscopy measurement. Y. L. helped with catalyst measurement. P.M. helped with real sunlight spectrum

estimation. K.P. helped with HPLC measurement. C.L., A.B.B. and Y.C. analyzed the data and co-wrote the paper. All the authors discussed the whole paper.

Competing Financial Interests

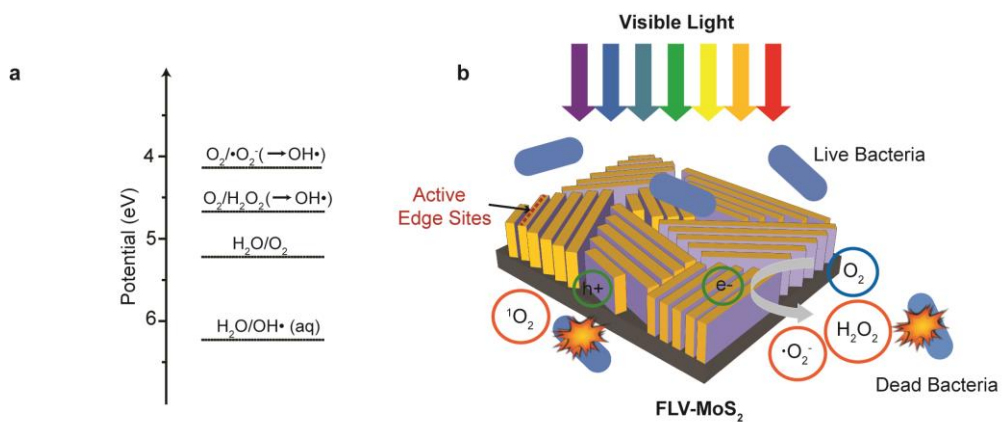The authors declare no competing financial interest.

Figures and Legends

Figure 1 | FLV-MoS$_2$ disinfection schematic. a, The ROS formation potentials with respect to vacuum level. **b**, Schematic showing FLV-MoS$_2$ inactivating bacteria in water through visible light photocatalytic ROS generation.
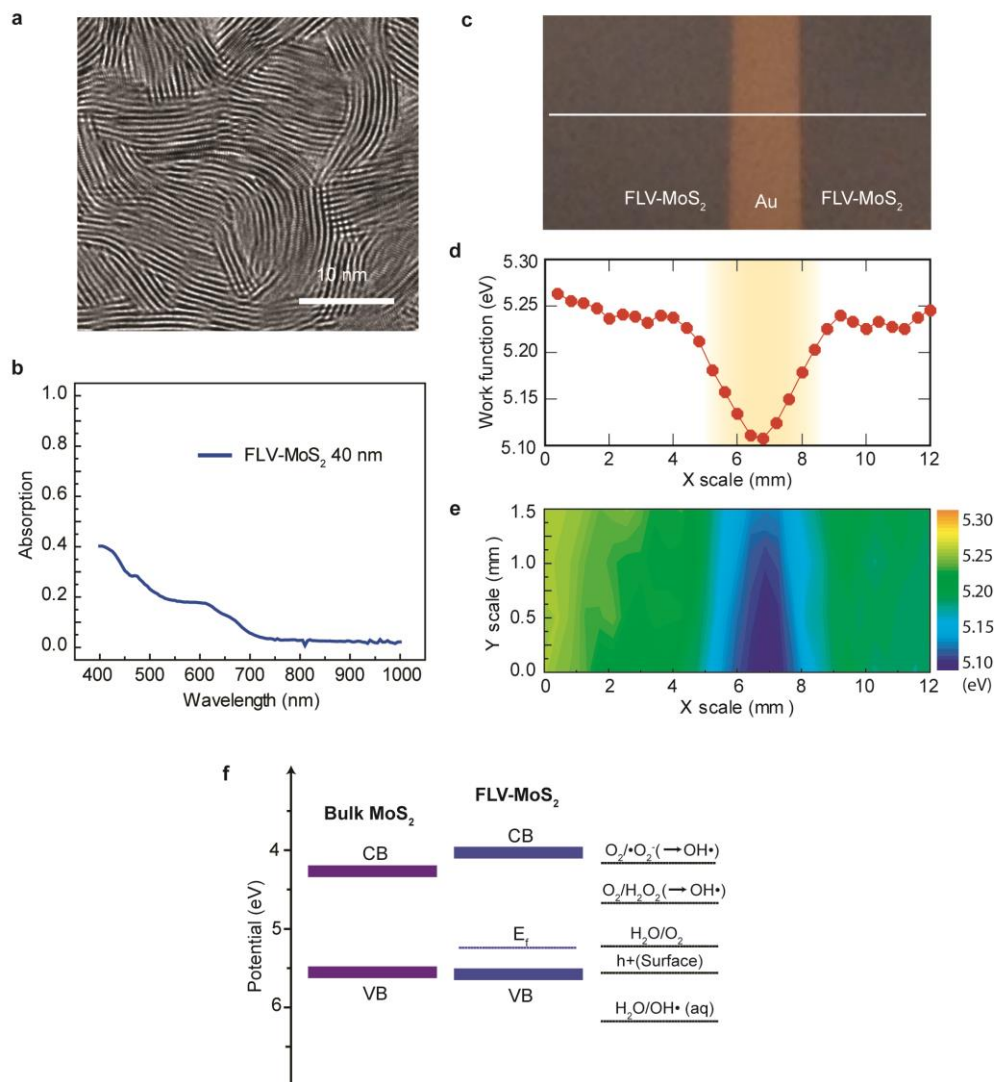
Figure 2 | FLV-MoS₂ morphology and band structure characterization. a, Top view TEM image of FLV-MoS₂ showing the as-grown vertically standing layers. **b**, Absorption spectrum of 40 nm FLV-MoS₂. **c**, Photograph of the FLV-MoS₂ film patterned with Au line for scanning KP measurement. **d**, Line scale data showing the fermi level of FLV-MoS₂ at each position on the white line in **c**. **e**, Mapping of the FLV-MoS₂ film showing the fermi level of each point on the film. **f**, The band position of FLV-MoS₂ with respect to ROS formation potential and bulk MoS₂ band position.
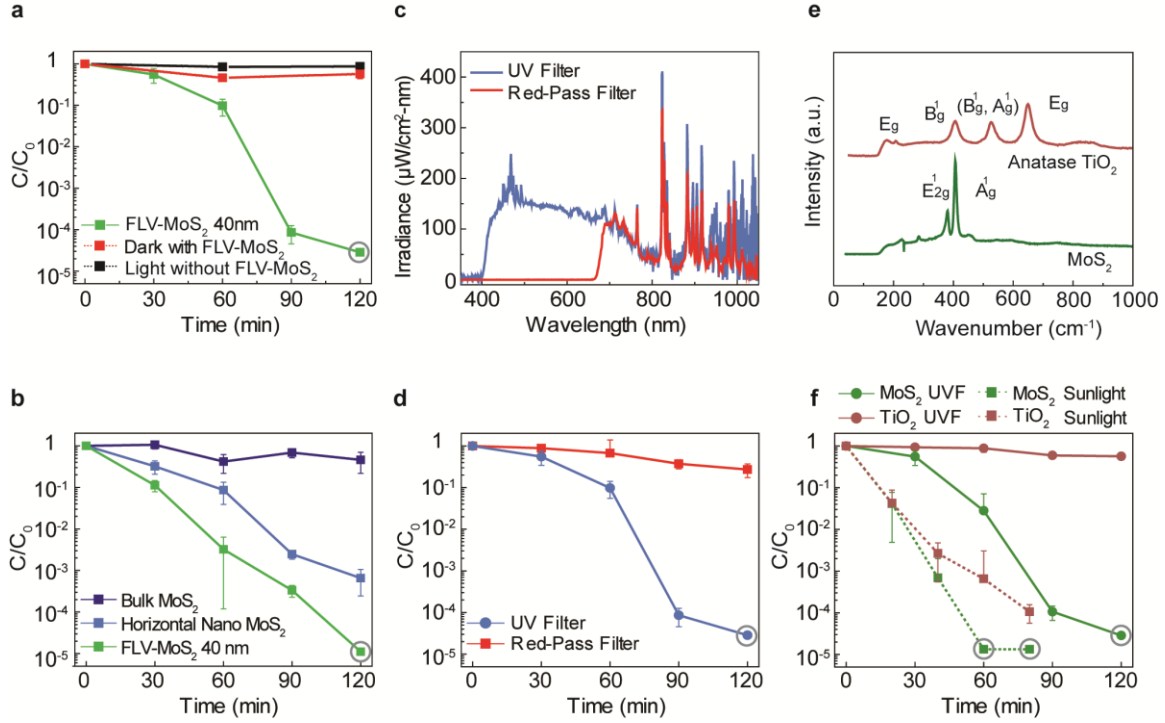
Figure 3 | FLV-MoS₂ disinfection performance. a, Comparison of disinfection performances of FLV-MoS₂ to light control without FLV-MoS₂ and FLV-MoS₂ in dark to confirm the visible light photocatalytic effect. **b**, Disinfection performances of FLV-MoS₂ compared with horizontal nano MoS₂ and bulk MoS₂. **c**, Spectrums of illuminating light sources, solar simulator with UV filter and solar simulator with red-pass filter. **d**, Disinfection performances using different light sources, solar simulator with UV filter and solar simulator with red-pass filter. **e**, Raman spectra of FLV-MoS₂ and TiO₂ films. **f**, Comparison of disinfection performance between FLV-MoS₂ and TiO₂ films under both visible light and real sunlight illumination. In the disinfection performances, error bars represent the standard deviation of three replicate measurements and data point with grey circle means no live bacteria was detected.
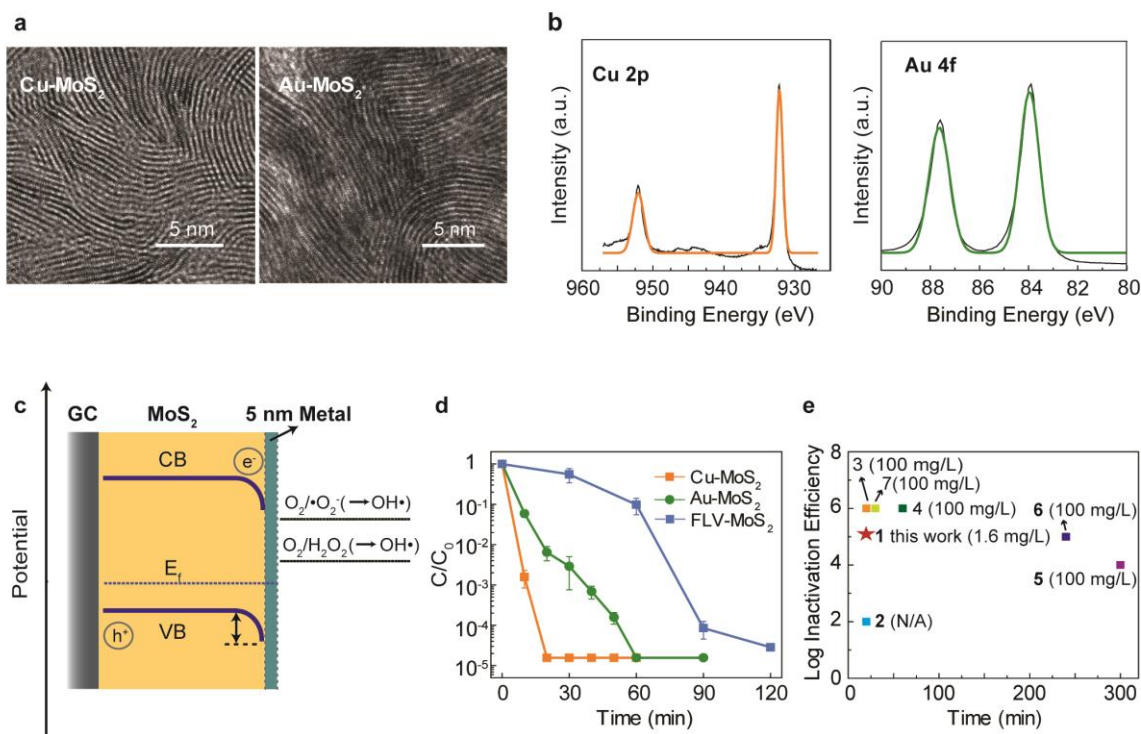
Figure 4 | Performance enhancement of FLV-MoS$_2$ by 5 nm of catalysts of Cu or Au. a, Top view TEM images showing the morphology of Cu-MoS$_2$ and Au-MoS$_2$ after deposition. **b**, XPS characterization of Cu-MoS$_2$ and Au-MoS$_2$ showing the presence of Cu and Au. **c**, Schematic showing the enhancement of electron-hole separation to facilitate the electrons to participate in ROSs generation reactions after Cu/Au deposition. **d**, Disinfection performance comparison of Cu-MoS$_2$ and Au-MoS$_2$ to pristine FLV-MoS$_2$ showing the rapid disinfection by Cu-MoS$_2$ and Au-MoS$_2$ after deposition of catalysts. **e**, Disinfection performance comparison of Cu-MoS$_2$ with other photocatalysts using *E. coli* from the literature. Plot shows the log inactivation of *E. coli* with respect to illumination time for all photocatalysts in comparison: 1. Cu-MoS$_2$ (this work, 2 cm^2 film equivalent to 1.6 mg/L), 2. TiO$_2$-CdS[25] (1 cm^2 film), 3. ZnO/Cu[48] (100 mg/L), 4. GO-CdS[34] (100 mg/L), 5. BV[36] (100 mg/L), 6. GO-C$_3$N$_4$[37] (100 mg/L) and 7. SGO-ZnO-Ag[35] (100 mg/L). Details for photocatalytic disinfection experiment conditions (sample concentration, light source and intensity and bacteria strain) are shown in Supplementary Table 1. The final inactivation efficiencies are limited by the initial bacterial concentration.

Methods

FLV-MoS$_2$ growth. Edge-terminated MoS$_2$ films are grown inside a single-zone, 12-in. horizontal tube furnace (Lindberg/Blue M) equipped with a 1-in.-diameter quartz tube. For 40 nm FLV-MoS$_2$ film, the substrates (1 cm$\times$2 cm) were sputtered with 10-nm-thick Mo film as a precursor and then sulfurization at a base pressure of 100 mTorr Ar environment. The tube furnace was quickly raised to reaction temperature of 500 °C in 20 min and kept at 500 for 10 min for reaction[41].

Disinfection performance. Bacteria, *Escherichia coli* (JM109, Promega and ATCC K-12) and *Enterococcus faecalis* (ATCC 19433), were cultured to log phase, harvested by centrifugation at 900$\times$g, washed twice with DI water and suspended in DI water to ~10^6 CFU/mL. Photocatalytic disinfection was performed using solar simulator (Newport) calibrated as AM1.5 (100 mW/cm^2) as light source and UV filter (Clarex) and red-pass filter (Clarex NIR-70) to tune the light spectrum. FLV-MoS$_2$ sample size is 1 cm $\times$ 2 cm $\times$ 40 nm and water volume is 25 mL. Bacterial concentrations were measured at different time of illumination using standard spread plating techniques. Each sample was serially diluted and each dilution was plated in triplicate onto trypticase soy agar and incubated at 37°C for 18 h. The solar disinfection performance experiments were conducted in duplicate. The light spectrums (solar simulator with UV filter or solar simulator with red-pass filter) were measured at the same place where the sample was set during the disinfection experiment. The solar spectrum during the real sunlight experiment was estimated using simple model of the atmospheric radiative transfer of sunshine (SMARTS). Disinfection rates (k) were estimated using Chicks law: $\ln(C/C_0) = -kt$ where k is in units of per time, C is the concentration of bacteria and C_0 is the concentration at t=0 of the experiments. The slope of the best fit line to $\ln(C/C_0)$ versus t for each experiment was used to estimate k.

Material Characterization. Characterizations were carried out using TEM (aberration-corrected FEI 80-300 environmental Titan (S) TEM microscope at 300 keV), Raman spectroscopy (WITEC Raman spectrometer), X-ray photoelectron spectroscopy (XPS, SSI SProbe XPS spectrometer with Al (Ka) source), scanning electron microscopy (SEM, FEI Nova NanoSEM 450), and scanning Kelvin probe (KP Technology Model 5050). The absorption measurement was using a xenon lamp (69911, Newport) as the light source coupled with a monochromator (74125, Newport).